Epitaxial strain effect on the $J_{\text{eff}} = 1/2$ moment orientation in Sr_2IrO_4 thin films

Ludi Miao,[1] Hong Xu,[1,2] and Z. Q. Mao[1,*]

[1]*Department of Physics and Engineering Physics, Tulane University, New Orleans, Louisiana 70118, USA*

[2]*Institute of Laser Engineering, Beijing University of Technology, Beijing 100124, P.R. China*

(Received 18 September 2013; revised manuscript received 16 December 2013; published 8 January 2014)

We have grown Sr_2IrO_4 (SIO) epitaxial thin films on $SrTiO_3$ (STO) and $NdGaO_3$ (NGO) substrates by a pulsed laser deposition method and characterized their structures and magnetic properties. We find that SIO films grown on STO substrates display tetragonal structure with a tensile strain of 0.13%, while SIO films grown on NGO substrates exhibit slightly orthorhombic structure with anisotropic biaxial tensile strains of 0.39% and 0.51% along the in-plane crystallographic axes. Although both films display insulating properties as bulk SIO does, their magnetic properties are distinct from that of bulk SIO. The ferromagnetic (FM) component of the $J_{\text{eff}} = 1/2$ canted antiferromagnetic order, which emerges below ~240 K in bulk SIO, is significantly weakened in both films, with a greater weakening appearing in the SIO/NGO film. From structural and magnetoresistance anisotropy analyses for both films, we reveal that the weak FM component in SIO films is dependent on the epitaxial strain. The greater tensile strain leads to a smaller octahedral rotation: The rotation angle is ~9.7(1)° for the SIO/NGO film and ~10.7(2)° for the SIO/STO film. These findings indicate that the $J_{\text{eff}} = 1/2$ moment orientation in SIO follows the IrO_6 octahedral rotation due to strong spin-orbit interaction.

DOI: 10.1103/PhysRevB.89.035109 PACS number(s): 73.50.−h, 68.55.−a, 75.70.Tj, 71.27.+a

I. INTRODUCTION

Transition metal oxides (TMOs) have been a fertile ground for condensed matter physics due to their fascinating exotic phenomena such as high-temperature superconductivity in cuprates [1–2], spin triplet superconductivity in ruthenates [3–5], colossal magnetoresistance in manganites [6], and metal-insulator transition in vanadates [7]. These physical properties are extremely sensitive to the external stimuli such as magnetic field [8], lattice distortion [9–10], and carrier doping [11] due to the complex interplay among the spin, charge, lattice, and orbital degrees of freedom. Recently, 5*d* TMOs such as iridates have drawn great attention due to the new physics arising from the large relativistic spin-orbit interaction (SOI) in heavy elements [12–15]. The strength of SOI λ_{S-O} is as large as 0.4 eV, comparable to the kinetic energy and the Coulomb repulsion energy in 5*d* TMOs. Such strong SOI in 5*d* TMOs is expected to lead to new exotic phases not seen in the 3*d* and 4*d* TMOs, such as topological insulating states [16–19], a Weyl semimetal [20–21], and an axion insulator [22].

Single-layered perovskite Sr_2IrO_4 (SIO) is a good example that has attracted a great deal of interest in SOI physics. Due to the spatially extended 5*d* orbits, the Coulomb repulsion U becomes very small. Based on the traditional Mott physics, SIO is expected to be a Fermi liquid metal like its 4*d* counterpart Sr_2RhO_4 [23]. Surprisingly, SIO is found to be a Mott insulator [24]. This puzzle can be solved only by taking the strong SOI into consideration [12]. In such a case, spin and orbital moments alone are no longer good quantum numbers, yet the total moment J is still a good quantum number. The originally degenerated t_{2g} band is split up into a narrower, half-filled $J_{\text{eff}} = 1/2$ band and a wider, filled $J_{\text{eff}} = 3/2$ band. The $J_{\text{eff}} = 1/2$ band is so narrow that even the weak Coulomb repulsion U is sufficient to open up a gap, establishing a novel $J_{\text{eff}} = 1/2$ Mott state. The existence of the $J_{\text{eff}} = 1/2$ Mott state has been proven by resonant x-ray scattering measurement [25]. The $J_{\text{eff}} = 1/2$ moments form a canted antiferromagnetic (AFM) order with $T_N \sim 240$ K, leading to a weak ferromagnetic (FM) behavior that appears at T_N [24,26]. The origin of moment canting is attributed to the Dzyalosinsky-Moriya (DM) interaction, which originates from the absence of the inversion symmetry of adjacent AFM coupled spins [24,27,28]. The structural inversion symmetry breaking in SIO is caused by the rotation of IrO_6 octahedra about the *c*-axis [24]. Another alternate explanation for the moment canting in SIO is that the strong SOI locks the relative orientation of spin and orbital moments, such that the total moment J is frozen in the IrO_6 octahedral cage and forced to rotate together with the IrO_6 octahedron [29]. Indeed, recent resonant x-ray scattering measurements by Boseggia *et al.* [30] show that in SIO, the IrO_6 octahedra rotation angle [11.8(1)°] is very close to the $J_{\text{eff}} = 1/2$ moment canting angle [12.2(8)°], suggesting that the $J_{\text{eff}} = 1/2$ moments are rigidly locked to the correlated rotations of IrO_6 octahedra [30].

Given that SIO exhibits a novel, SOI-driven Mott state, the tuning of the SIO ground state may lead to new exotic phases characterized by high-temperature superconductivity [31]. Indeed, the physical properties of SIO have been shown to be tunable by chemical doping, quasihydrostatic pressure, and epitaxial strain. One example is the $Sr_2Ir_{1-x}Rh_xO_4$ system, where the iso-electronic doping of Rh does not change the lattice structure nor the Fermi level, but only suppresses the SOI [32–33]. Optical spectrum measurements revealed that the Mott gap of SIO thin film collapses upon Rh substitution [32]. Indeed, only 7% doping of Rh can effectively decrease the resistivity of the system by six orders of magnitude [33]. Secondly, the quasihydrostatic pressure was found to cause a striking effect on the magnetic properties of SIO; the weak FM component is quenched under a pressure above 17 GPa, which is believed to result from the tetragonal distortion of IrO_6 octahedra induced by the pressure [34]. Another example is the epitaxial SIO thin film system [35–36], where the IrO_6

*Corresponding author: zmao@tulane.edu

octahedral rotation and interlayer spacing are controlled by the epitaxial strain [35]. Optical spectroscopy studies on such films clearly indicate that the electronic state is tuned by the epitaxial strain [35], and transport measurements reported by Rayan-Serrao *et al*. [36] show that the energy gap size of SIO film can be modified by the strain. However, the effect of the epitaxial strain on the magnetic order of SIO is yet to be investigated.

Given that the weak FM behavior of SIO originates from the lattice distortion through the DM interaction [24], the epitaxial strain may cause significant influence on the magnetism of the SIO films. To investigate the strain effect on the magnetism of SIO, we have grown SIO epitaxial thin films on perovskite substrates of $SrTiO_3$ (STO) and $NdGaO_3$ (NGO) using a pulsed laser deposition (PLD) method. In this paper, we report the structural, magnetic, and magnetotransport properties of SIO thin films. The SIO/STO film exhibits an isotropic tensile strain of 0.13%, whereas the SIO/NGO film exhibits an anisotropic biaxial tensile strain of 0.39% and 0.51% along the two in-plane crystallographic axes, respectively. Our systematic magnetoresistance (MR) measurements reveal that the FM behavior is much more significantly weakened in the SIO/NGO film than in the SIO/STO film. We will show that the distinct magnetic behaviors between these two types of films can be well understood in terms of the dependence of the $J_{\text{eff}} = 1/2$ moment orientation on the epitaxial strain.

II. EXPERIMENT

We have grown epitaxial thin films of SIO using the PLD method with a KrF excimer laser ($\lambda_{\text{PLD}} = 248$ nm). Single crystalline STO and NGO are used as substrates, both with (001) pseudocubic orientations. A stoichiometric SIO polycrystalline pellet was used as the target. The SIO films were deposited at 1080°C in an atmosphere of 150 mTorr of O_2. The thickness of SIO films used for current studies is 200 nm. We chose to use such thick films for the following reasons: (a) Since SIO films exhibit insulating behavior, their in-plane resistances are extremely large at low temperatures. For example, the 10-nm-thick SIO film yields a resistance larger than 10^{11} Ω at low temperatures, which is beyond our measurement limit. (b) The resistances of 200 nm films are within the measurable range, even at low temperatures. (c) SIO/STO and SIO/NGO films are distinctively strained in spite of the 200 nm thickness, as shown below. The structures of films were characterized by a high-resolution four-circle x-ray diffractometer (HR-XRD, Bruker) with a Cu K-α1 radiation of wavelength $\lambda_{\text{XRD}} = 1.5406$ Å; magnetic properties of films were probed by a superconducting quantum interference device (SQUID, Quantum Design). Their electronic transport properties were measured using a standard four-probe method in a physical property measurement system (PPMS, Quantum Design).

III. RESULTS AND DISCUSSIONS

Fig. 1(a)–1(f) presents the HR-XRD data for SIO films on STO and NGO substrates, respectively. The strong (00l) diffraction peaks in the θ–2θ scans shown in Fig. 1(a) and 1(b) confirm high crystalline quality with c-orientation for

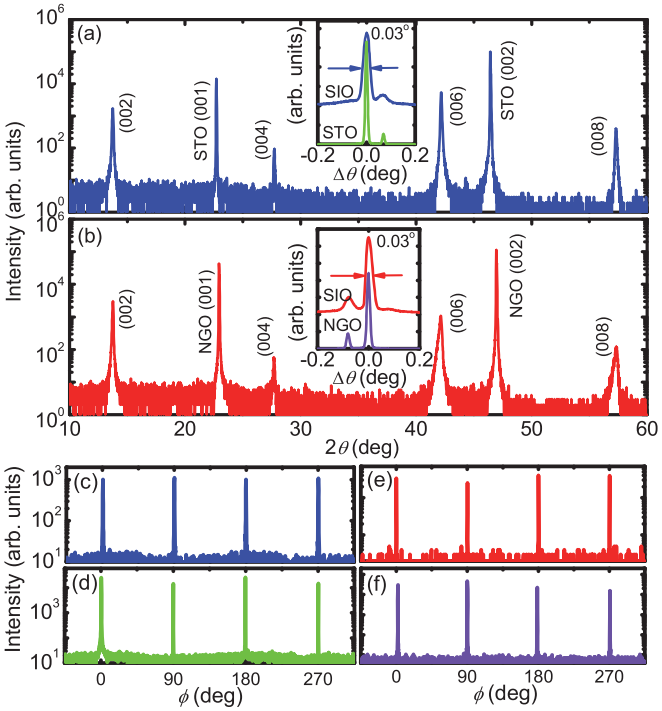

FIG. 1. (Color online) HR-XRD θ–2θ scans of 200 nm SIO films on (a) STO and (b) NGO substrates. The insets show the rocking curves of (002) reflections around the SIO films and corresponding substrates (the data have been shifted for clarity). ϕ scans of (c) SIO (103), (d) STO (101) reflections for the SIO/STO film, (e) SIO (103), (f) NGO (101) reflections for the SIO/NGO film. $\phi = 0°$ is defined as the direction parallel to $[100]_{\text{STO}}$ or $[100]_{\text{NGO}}$.

both films. The sharp rocking curves of SIO (002) peaks, with the full widths at half maximum (FWHMs) as sharp as 0.03° (see the insets), indicate both films exhibit very small mosaic spread. The satellite peaks near the SIO (002) reflections in the rocking curves for both films are attributed to other domains in the films, which arise from the multiple domains of the commercial substrates, as confirmed by the rocking curves of STO (002) and NGO (002) reflection peaks, shown in the insets of Fig. 1(a) and 1(b), respectively. From the XRD ϕ-scans for STO (101), NGO (101), and SIO (103) reflection peaks shown in Fig. 1(c)–1(f), fourfold symmetries are observed, indicating the epitaxial growth with $[100]_{\text{SIO}}\|[100]_{\text{STO}}$, $[010]_{\text{SIO}}\|[010]_{\text{STO}}$, and $[001]_{\text{SIO}}\|[001]_{\text{STO}}$ for the SIO/STO film and $[100]_{\text{SIO}}\|[100]_{\text{NGO}}$, $[010]_{\text{SIO}}\|[010]_{\text{NGO}}$, and $[001]_{\text{SIO}}\|[001]_{\text{NGO}}$ for the SIO/NGO film, respectively. The diffraction indices denoted in Fig. 1 are based on the pseudotetragonal unit cell with $a \approx b \approx a_0/\sqrt{2}$, $c = c_0/2$ for SIO (where $a_0 = \sqrt{2} \times 3.888$ Å and $c_0 = 2 \times 12.899$ Å are lattice constants of bulk SIO [24]), and the pseudocubic unit cell with $a_{\text{NGO}} = c_{\text{NGO}} \approx a_{\text{NGO0}}/\sqrt{2}$ and $b_{\text{NGO}} = c_{\text{NGO0}}/2$ for NGO (where $a_{\text{NGO0}} = 5.431$ Å, $b_{\text{NGO0}} = 5.499$ Å, and $c_{\text{NGO0}} = 7.557$ Å are lattice constants of orthorhombic NGO).

We have also performed XRD reciprocal space map (RSM) measurements on the SIO films in order to determine their in-plane lattice constants, as shown in Fig. 2(a) and 2(c)–2(f). Although the SIO films involve multiple domains, only the major one is probed in the RSMs, indicated by the single

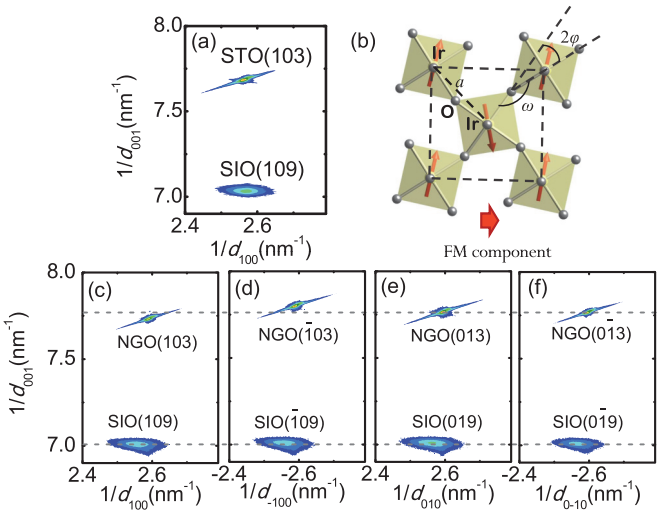

FIG. 2. (Color online) Reciprocal space maps of HR-XRD around the (a) STO (103) and SIO (109), (c) NGO (103) and SIO (109), (d) NGO (−103) and SIO (−109), (e) NGO (013) and SIO (019), (f) NGO (0–13) and SIO (0–19) peaks. (b) Schematic diagram of SIO in-plane structure; a, in-plane lattice constant; ω, the in-plane Ir-O-Ir bond angle; φ, the IrO_6 octahedral rotation angle. The horizontal arrows represent the ferromagnetic component from canted $J_{\text{eff}} = 1/2$ moments.

(109) diffraction spot of the SIO film. The SIO/STO film possesses a tetragonal structure due to the cubic lattice of STO, while the SIO/NGO film lattice has a slightly orthorhombic distortion due to the monoclinic lattice of NGO, for which a two-dimensional surface lattice is expected to be rectangular. For the tetragonal SIO/STO film, the lattice parameters a and c are determined to be 3.893 Å and 12.796 Å, respectively, from the horizontal and vertical peak positions of the (109) diffraction spot in the RSM shown in Fig. 2(a). For the SIO/NGO film, however, at least two RSMs around (109) and (019) reflections of SIO are required to determine the a, b, and c lattice constants of the orthorhombic lattice. Moreover, given that the NGO substrate is monoclinic, one should rule out the possibility that the SIO film possesses a monoclinic lattice. To verify the orthorhombicity of the SIO film, we need four RSMs around (109), (019), (−109), and (0–19) reflections of SIO; these RSMs are shown in Fig. 2(c)–2(f). The $1/d_{001}$ values of the (103), (−103), and (013) reflections of NGO are all different, whereas those of the (013) and (0–13) reflections of NGO are the same (see the dashed eye guideline), reflecting the fact that $\beta \neq 90°$ and $\alpha = 90°$ for the NGO lattice, respectively. In contrast, the $1/d_{001}$ values of all four SIO reflection spots are the same (see the dashed eye guideline), indicating that $\alpha = \beta = 90°$ for the SIO lattice. Given that the two-dimensional surface lattice of the NGO substrate is rectangular, the SIO film should exhibit peak splitting in RSM if $\gamma \neq 90°$, due to possible twin domains. However, the absence of SIO peak splitting indicates that $\gamma = 90°$ for the SIO lattice. Therefore, the SIO/NGO film should possess an orthorhombic lattice. From the horizontal and vertical positions of the (109), (019), (−109), and (0–19) reflections in the RSMs, a, b, and c lattice constants are calculated to be 3.903 Å, 3.908 Å, and 12.839 Å, respectively, for the SIO/NGO film.

Based on the bulk SIO lattice constants $a_0 = \sqrt{2} \times 3.888$ Å and $c_0 = 2 \times 12.899$ Å, together with the lattice constants of SIO films we calculated from RSM results, we can evaluate the epitaxial strains for the SIO films along in-plane crystallographic directions, which are defined as $\varepsilon_a = \frac{\sqrt{2}a - a_0}{a_0}$ and $\varepsilon_b = \frac{\sqrt{2}b - b_0}{b_0}$. The SIO/STO film is under an isotropic biaxial tensile strain with $\varepsilon_a = \varepsilon_b = 0.13\%$. This tensile strain agrees with the fact that the d_{110} of the STO substrate ($= \sqrt{2} \times 3.905$ Å) is larger than the in-plane lattice constant of bulk SIO. Since the probed strain (0.13%) is less than the expected full strain (0.44%), the strain is partially relaxed, which is understandable given the 200 nm film thickness. For the SIO/NGO film, since the lattice constants of NGO ($a_{\text{NGO}} = 3.855$ Å and $b_{\text{NGO}} = 3.864$ Å) are both smaller than those of bulk SIO, one would expect biaxial compressive strain along both in-plane directions. However, the SIO/NGO film is found to be under an anisotropic biaxial tensile strain with $\varepsilon_a = 0.39\%$ and $\varepsilon_b = 0.51\%$. Such a controversy between lattice mismatch and actual strain effect is also observed by Nicoles *et al.* in the SIO/$(LaAlO_3)_{0.3}(Sr_2AlTaO_6)_{0.7}$ film [35].

Since previous studies on SIO films have revealed that in-plane Ir-O bond lengths $d_{\text{Ir-O}}$ are rigid against the epitaxial strain, and the modification of in-plane lattice constants can be accommodated only by the change of in-plane Ir-O-Ir bond angle ω (see Fig. 2[b]) [35–36], we can expect that a different strain effect in SIO/STO and SIO/NGO films would result in distinct IrO_6 octahedral rotations. As shown in Fig. 2(b), the in-plane Ir-O-Ir bonding angle ω could be inferred from the Ir-O bond length and the in-plane lattice constant via $a = d_{\text{Ir-O}}\sqrt{2(1 - \cos\omega)}$ [35], and the IrO_6 octahedral rotation angle φ is equal to $(1/2)(180° - \omega)$. We estimate the IrO_6 octahedral rotation angles of SIO films using these relations and the lattice constants of SIO films probed in RSMs in Fig. 2. The value for φ is $\sim 10.7(2)°$ for the SIO/STO film and 9.7(1)° for the SIO/NGO film. Both are smaller than $\varphi = 11.8(1)°$ for the bulk SIO [30], consistent with our conjecture. Given that our SIO films have 200 nm thickness, a natural question is whether the decreased rotation angles of IrO_6 octahedra in our SIO films extend through the entire thickness. Since the increased lattice parameter a probed by the XRD-RSM measurements is an average effect of entire thickness, we can reasonably expect that the decrease of the octahedral rotation extends through the whole thickness on the average. Since the weak FM behavior in SIO is caused by the $J_{\text{eff}} = 1/2$ moment canting, which is rigidly locked to IrO_6 octahedral rotation through the DM interaction, as indicated above [24,30], the smaller IrO_6 octahedral rotation angles in SIO films are expected to result in weakened FM behavior. This is exactly what we observed in our experiments, as shown below.

We present in-plane resistivity (ρ_{ab}) as a function of temperature (T) for both SIO/STO and SIO/NGO films in Fig. 3(a). Both films exhibit insulating behavior in the whole measured temperature range, which implies that they are still in the $J_{\text{eff}} = 1/2$ Mott insulating state like the bulk SIO, consistent with the result reported by Rayan-Serrao *et al.* [36]. Figure 3(b) shows the magnetization as a function of

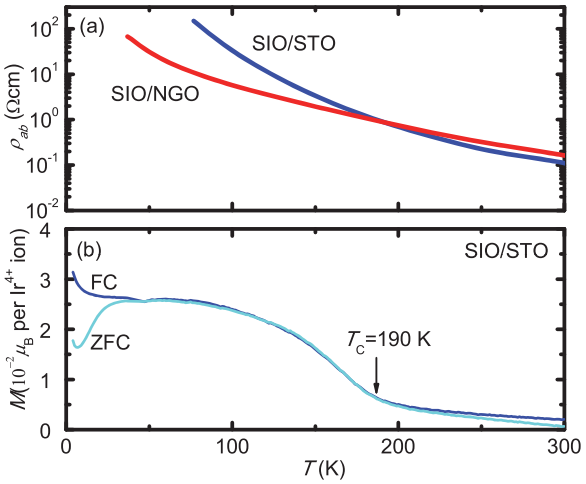

FIG. 3. (Color online) (a) In-plane resistivity vs. temperature for SIO films. (b) Magnetization as a function of temperature for the SIO/STO film, measured with the magnetic field of 5 kOe applied along $[100]_{SIO}$ and ZFC and FC histories.

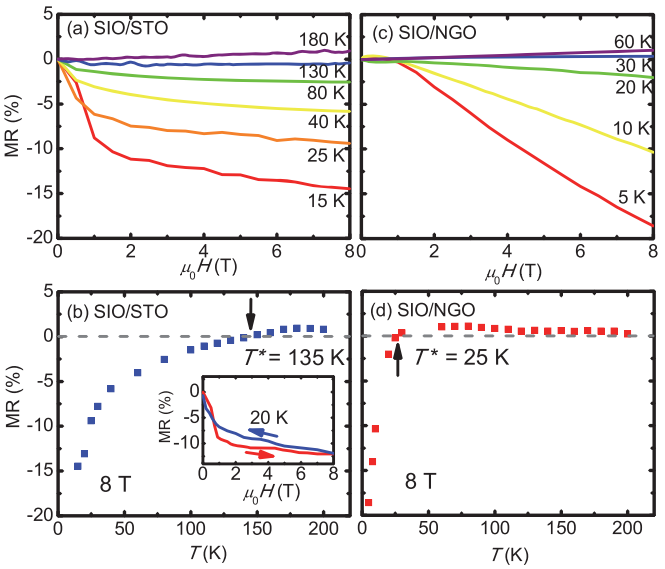

FIG. 4. (Color online) Magnetoresistance (MR) vs. magnetic field (along $[100]_{SIO}$) at various fixed temperatures for the (a) SIO/STO film and the (c) SIO/NGO film. MR at 8 T as a function of temperature for the (b) SIO/STO film and the (d) SIO/NGO film. The inset of (b) shows MR vs. magnetic field at 20 K for the SIO/STO film.

temperature $M(T)$ for the SIO/STO film measured under a field of 5 kOe along $[100]_{SIO}$. The diamagnetic contribution from the STO substrate, measured separately after grinding off the film from the substrate, has been subtracted from the overall magnetization. The weak FM behavior below T_C = 190 K apparently arises from the moment canting in the AFM order as indicated above [24]. The irreversibility observed below T_{ir} = 36 K between the zero-field-cooling (ZFC) and the field-cooling (FC) histories represents low-temperature enhancement of the FM component due to the decrease of thermal fluctuations. In comparison with the SIO bulk, which shows a weak FM component below $T_C \sim 240$ K and irreversibility of magnetization below $T_{ir} \sim 180$ K (probed at 5 kOe) [37], the FM component in the SIO/STO film is indeed weakened, as we expected. However, since the paramagnetic signal of NGO substrate is three orders of magnitude larger than that of the SIO film, we could not examine the magnetic properties for the SIO/NGO film directly from magnetization measurements.

To examine the magnetic properties of the SIO/NGO film and compare it with those of the SIO/STO film, we performed magnetotransport measurements for both films. In Fig. 4(a) and 4(c), we show the in-plane magnetoresistance, $MR = \frac{\rho_{ab}(H)-\rho_{ab}(0)}{\rho_{ab}(0)}$, as a function of field H (along $[100]_{SIO}$) at various temperatures, for the SIO/STO and the SIO/NGO films. One remarkable feature for the SIO/STO film is that its MR measured under a field of 8 T undergoes a transition from positive to negative on cooling at $T^* = 135$ K, as shown in Fig. 4(b). Below ~40 K, MR tends to saturate when the applied field is increased above 1 T and shows hysteresis behavior between upward and downward field sweeps at 20 K, as shown in the inset of Fig. 4(b). Apparently, these characteristics agree well with the low-temperature enhanced FM component from the canted AFM order due to the decrease of the thermal fluctuations. This observation is also in line with the magnetotransport properties of bulk SIO, which exhibits negative MR with saturation and hysteresis behavior at low temperatures [29]. The MR of the SIO/NGO film measured under a field of 8 T also exhibits a positive-to-negative transition, but at a much lower temperature $T^* = 25$ K, as shown in Fig. 4(d). However, the low-temperature saturation behavior seen in the MR(H) curves for the SIO/STO film is absent for the SIO/NGO film [see Fig. 4(c)], indicating that the FM component in the SIO/NGO film is more heavily weakened as compared to the SIO/STO film.

Stronger weakening of FM component in the SIO/NGO film is also evidenced in the measurements of angular dependence of magnetoresistance (AMR) for the SIO/STO and the SIO/NGO films. The schematic diagram of the AMR measurement setup is shown in Fig. 5(a). In Fig. 5(b)–5(e), we present AMR as a function of polar angle θ measured at a fixed field $\mu_0 H = 8$ T and using various temperatures for the SIO/STO and the SIO/NGO films. Here, AMR is defined as $\mathrm{AMR}(\theta,T) = \frac{\rho_{ab}(H,\theta,T)-\rho_{ab}(0,T)}{\rho_{ab}(0,T)}$, where the orientation angle θ of the magnetic field and temperature are variables. For the SIO/STO film, AMR shows a strong twofold periodicity with the minimum value along the in-plane direction when $T<T^*$ (=135 K). As indicated above, the low-temperature enhanced FM component is responsible for the negative MR in the SIO/STO film through the spin scattering mechanism. The observation of AMR minimum value along the in-plane direction is consistent with the in-plane–oriented FM component arising from the $J_{\mathrm{eff}} = 1/2$ moment canting [24–25]. However, when the temperature is increased above T^*, where MR becomes positive, although AMR shows twofold anisotropy, the minimum value switches to the out-of-plane direction. Moreover, the magnitude of MR is also much smaller for $T>T^*$ than for $T<T^*$. The SIO/NGO film also shows a sign reversal in MR, but at a much lower temperature T^* (=25 K), as indicated above. Like the SIO/STO film, the SIO/NGO film also exhibits a weak twofold anisotropy in its AMR, with the

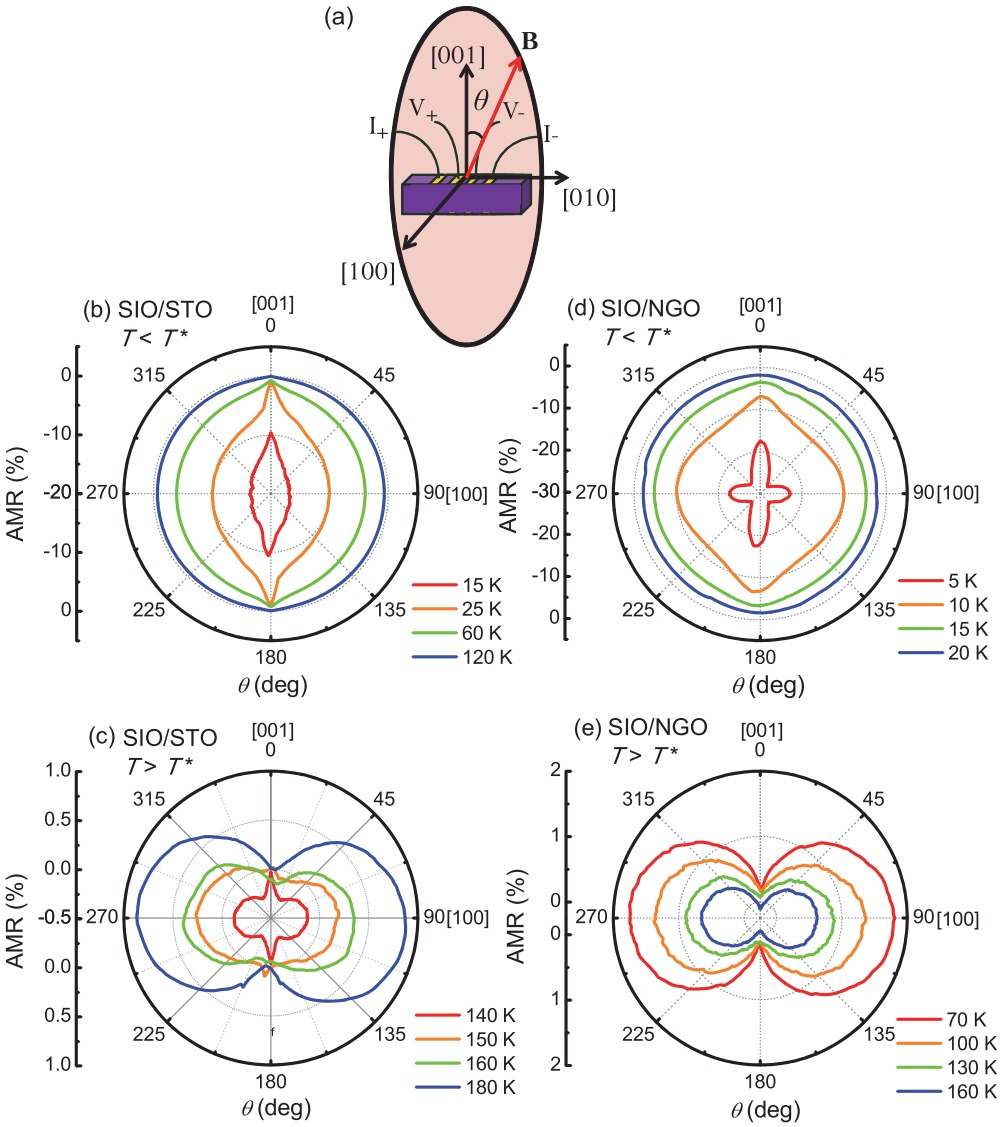

FIG. 5. (Color online) (a) Schematic diagram of magnetic field orientation relative to crystallographic axes in AMR measurements, with the polar angle θ denoting the direction of magnetic field. Polar angular dependence of normalized in-plane magnetoresistance $\text{AMR}(\theta,T) = \frac{\rho_{ab}(H,\theta,T)-\rho_{ab}(0,T)}{\rho_{ab}(0,T)}$ for the SIO/STO film for (b) $T < T^* = 135$ K and (c) $T > T^* = 135$ K, for the SIO/NGO film for (d) $T < T^* = 25$ K and (e) $T > T^* = 25$ K. All the data in (b)–(e) are collected at a fixed field of 8 T. T^* represents the critical temperature for the sign reversal of MR (see text). MR is positive above T^* but negative below T^*.

minimum values along the out-of-plane direction for $T > T^*$. Nevertheless, at temperature below T^*, the SIO/NGO film shows distinct behavior in AMR from the SIO/STO film. Its AMR consists of two components, i.e., a dominating fourfold periodicity plus a minor twofold periodicity. The signature of double components becomes significant for $T < 10$ K. We notice that such an AMR anisotropy with double components looks similar to the anisotropic behavior of AMR in the SIO/$La_{2/3}Sr_{1/3}MnO_3$ (LSMO)/STO film recently reported by Marti *et al.* [38], where MR is measured with the current along the *c*-axis.

The distinct temperature dependence of AMR anisotropy between the SIO/STO and the SIO/NGO films implies that these two films have distinct magnetic properties. To further address this issue, we performed Fourier transformation analyses for the $\text{AMR}(\theta,T)$ data, from which we can obtain the *n*-fold Fourier complex amplitude A_n and normalized weight W_n as functions of temperature for both films, where $A_n(T) = \frac{1}{2\pi}\int_0^{2\pi} \text{AMR}(\theta,T)\exp(-in\theta)\text{d}\theta$ and $W_n(T) = |A_n(T)|^2 / \sum_n |A_n(T)|^2$. Figure 6(a) and (c) shows $\psi_2(T)$, the phase angle of $A_2(T)$ for SIO/STO and SIO/NGO films, which is determined by the AMR minimum value direction. For the SIO/STO film, $\psi_2(T)$ remains at constants of 0 and π for $T < T^*$ and $T > T^*$, indicating the AMR minimum values are along in-plane and out-of-plane directions for these temperature regions, respectively. The remarkable π phase shift in $\psi_2(T)$ across T^* ($= 135$ K) reflects the observed switching behavior of AMR minimum value directions at T^*. The value of $\psi_2(T)$ for the SIO/NGO film also exhibits a π phase shift, but at a much lower temperature, $T^* = 25$ K, where MR shows a sign reversal. Figure 6(b) and (d) shows $W_2(T)$ and $W_4(T)$ for the SIO/STO and SIO/NGO films. Generally,

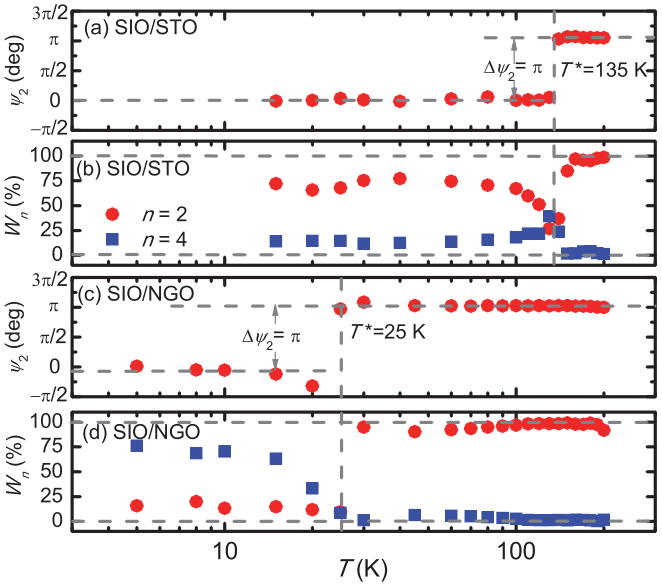

FIG. 6. (Color online) Phase angles ψ_2 of twofold Fourier amplitude A_2 of AMR(θ) of the (a) SIO/STO film and the (c) SIO/NGO film as a function of temperature at $\mu_0 H = 8$ T. Twofold squared weight W_2 and fourfold squared weight W_4, defined as $W_n(T) = |A_n(T)|^2 / \sum_n |A_n(T)|^2$, of the (b) SIO/STO film and the (d) SIO/NGO film as a function of temperature.

for a pure twofold anisotropy with $\sin(2\theta)$ angular dependence in MR, W_2 shows a value of 100%; however, if AMR involves a competition between two twofold components with different phase angles ψ_2, W_4 and even higher-order W_n ($n > 4$) show finite values. In this case, when the sum of W_n is normalized to unity, we can expect a deviation of W_2 from 100%. For the SIO/STO film, W_2 sharply increases above T^* and eventually reaches almost 100% for $T > 160$ K, indicating a pure twofold behavior. Such a pure twofold anisotropy in MR is commonly seen in AFM insulators, such as Ca_2RuO_4 [39], $Pr_{1-x}Sr_xMnO_3$ [40], and $La_{2-x}Ce_xCuO_4$ [41],; it reflects the Ising anisotropy of AFM order and existence of magnetic scattering. However, for $T < T^*$ region, W_2 reaches only ~75% below 90 K, suggesting the competition between a dominating twofold component with $\psi_2 = 0$ and a weak twofold component with $\psi_2 = \pi$. Indeed, W_4 reaches a finite value of 14% in this temperature region. W_2 exhibits a greater deviation as the temperature approaches T^*, with a minimum value of 25% occurring at T^*. In contrast, W_4 shows a maximum value of 40% at T^*. These facts indicate that the competition between these two twofold components is the strongest at T^*. As indicated above, the twofold component with $\psi_2 = 0$ should clearly be attributed to the low-temperature enhancement of the FM component arising from the moment canting in the AFM order, since it occurs at the same temperature where MR shows a positive-to-negative sign reversal. For the SIO/NGO film, W_2 also reaches almost 100% for $T > T^*$, indicating a pure twofold anisotropy due to the insulating AFM phase. However, for $T < T^*$, W_2 decreases to ~15%, whereas W_4 increases, up to 75% for $T < 10$ K. Such a large deviation from a pure twofold anisotropy indicates that the twofold component with $\psi_2 = 0$ is much weaker in the SIO/NGO film than in the SIO/STO film, consistent with the expected heavier weakening of the FM component in this film. Our analyses clearly reveal that the FM component, which arises from the canting of moments, depends on the IrO_6 octahedral rotation, which is in turn determined by the epitaxial strain. In other words, the $J_{\text{eff}} = 1/2$ moment orientation in SIO follows the IrO_6 octahedral rotation. This argument is consistent with the results obtained in recent x-ray resonant scattering studies on SIO, which show that the canting of magnetic moments is locked to the octahedral rotation due to strong spin-orbital interaction [30].

As noted above, the AMR anisotropy of SIO/LSMO/STO film reported by Marti *et al.* [38] looks similar to that of our SIO/NGO film. This implies that the FM component in the SIO/LSMO/STO film is heavily weakened as well. The epitaxial strain should also be responsible for such a FM component weakening. The SIO layer in the SIO/LSMO/STO film is as thin as 6 nm, i.e., much thinner than our SIO films, the thicknesses of which are 200 nm. In general, the strength of epitaxial strain is thickness dependent. Indeed, this has been observed by Rayan-Serrao *et al.* for SIO/STO films [36]. They found that the tensile strain is around 0.23% for a 10-nm-thick film and reaches as high as 0.31% for a 5-nm-thick film, i.e., much larger than the 0.13% tensile strain of our SIO/STO film. From the above discussions on the effect of epitaxial strain on IrO_6 octahedral rotation, we can expect a much smaller IrO_6 octahedral rotation in the SIO/LSMO/STO film as compared to our SIO/STO film. As a result, it is not surprising to observe a strongly weakened FM component in the SIO/LSMO/STO film. Given that the FM component is controlled by the IrO_6 octahedral rotation, one might speculate that the FM component would diminish when the octahedral rotation could be fully suppressed. Bulk Ba_2IrO_4 (BIO) actually represents an example for such a scenario. In BIO, the IrO_6 octahedra do not involve any rotation, and its AFM order is indeed not accompanied by a FM component [42].

Finally, we turn to a comparison of the strain effect of SIO films with the quasihydrostatic pressure effect of bulk SIO. As noted above, in bulk SIO under a quasihydrostatic pressure above 17 GPa, the weak FM behavior is quenched [34]. This fact, at a first glance, appears to be not in line with our observation that the tensile strain, which is equivalent to a negative pressure, also weakens FM behavior heavily. To reconcile this inconsistency, the change in the c-lattice constant should also be taken into consideration, since the ideal $J_{\text{eff}} = 1/2$ state only exists in a system of cubic symmetry [43]. The elongation of IrO_6 octahedra along the c-axis must also affect magnetic properties. For bulk SIO under a quasihydrostatic pressure of 17 GPa, the relative lattice constants shrink along the a-axis and c-axis, $-\Delta a/a = 2.5\%$ and $-\Delta c/c = 2.1\%$, respectively. Although the shrink in the a-axis favors the FM component, as discussed above, the shrink in the c-axis suppresses the FM component [34]. The net result of the competition is that the weak FM behavior is quenched under a pressure over 17 GPa. In our SIO films, although the in-plane axes exhibit relative elongations with $\varepsilon_a = \varepsilon_b = 0.13\%$ for the SIO/STO film and $\varepsilon_a = 0.39\%$ and $\varepsilon_b = 0.51\%$ for the SIO/NGO film, the c-axis shows relative shrinking of 0.79% for the SIO/STO film and 0.47% for the SIO/NGO film. Both changes of in-plane and c-axis tend to weaken the FM

components in our SIO film. The shrinking of the c-axis alone, however, cannot explain the weakening of FM components in our SIO films, since the SIO/NGO film shows a relatively smaller shrinking of the c-axis than the SIO/STO film, but it exhibits a much more weakened FM component. Therefore, the modifications of the magnetic properties for SIO films still need to be understood in terms of the modification of the $J_{\text{eff}} = 1/2$ moment orientation by epitaxial strain.

IV. CONCLUSION

We have grown SIO epitaxial thin films on perovskite STO and NGO substrates using the pulsed laser deposition method and investigated the strain effect on their magnetic properties. The SIO film on the STO substrate shows a tetragonal structure with 0.13% isotropic tensile strain. The SIO film on the NGO substrate, however, is characterized by an orthorhombic structure with anisotropic biaxial tensile strain (0.39% along the a-axis and 0.51% along the b-axis). Our detailed structural analyses reveal that the IrO_6 octahedral rotation is modified by the strain. A greater strain leads to a smaller octahedral rotation angle. The octahedral rotation angles for the SIO/NGO and SIO/STO films are estimated to be 9.71° and 10.72°, respectively, which are both smaller than the rotation angle of 11.05° for bulk SIO. The epitaxial strain results in a remarkable effect on magnetic properties of SIO. From magnetization and magnetotransport measurements, we found that the weak FM behavior, which originates from the canted AFM order, is strongly weakened for both films, with a heavier weakening occurring in the SIO/NGO film. The fact that a smaller FM component comes with a smaller IrO_6 octahedral rotation clearly indicates an important fact—that the orientation of the $J_{\text{eff}} = 1/2$ moment orientation is locked to the IrO_6 octahedral rotation which reflects the important role played by the strong spin-orbit interaction in iridates.

ACKNOWLEDGMENTS

This research is supported by the US Department of Defense Army Research Office under Grant No. W911NF0910530 and the National Science Foundation under Grant No. DMR-1205469.

[1] M. K. Wu, J. R. Ashburn, C. J. Torng, P. H. Hor, R. L. Meng, L. Gao, Z. J. Huang, Y. Q. Wang, and C. W. Chu, Phys. Rev. Lett. **58**, 908 (1987).
[2] C. W. Chu, P. H. Hor, R. L. Meng, L. Gao, Z. J. Huang, and Y. Q. Wang, Phys. Rev. Lett. **58**, 405 (1987).
[3] A. P. Mackenzie and Y. Maeno, Rev. Mod. Phys. **75**, 657 (2003).
[4] K. D. Nelson, Z. Q. Mao, Y. Maeno, and Y. Liu, Science **306**, 1151 (2004).
[5] Y. Maeno, S. Kittaka, T. Nomura, S. Yonezawa, and K. Ishida, J. Phys. Soc. Jpn. **81** 011009 (2012).
[6] M. B. Salamon and M. Jaime, Rev. Mod. Phys. **73**, 583 (2001).
[7] F. J. Morin, Phys. Rev. Lett. **3**, 34 (1959).
[8] S. Jin, M. McCormarck, T. H. Tiefel, and R. Ramesh, J. Appl. Phys. **76**, 6929 (1994).
[9] S. Nakatsuji and Y. Maeno, Phys. Rev. Lett. **84**, 2666 (2000).
[10] F. Nakamura, T. Goko, M. Ito, T. Fujita, S. Nakatsuji, H. Fukazawa, Y. Maeno, P. Alireza, D. Forsythe, and S. R. Julian, Phys. Rev. B **65**, 220402 (2002).
[11] A. D. Caviglia, S. Gariglio, N. Reyren, D. Jaccard, T. Schneider, M. Gabay, S. Thiel, G. Hammerl, J. Mannhart, and J. M. Triscone, Nature **456**, 624 (2008).
[12] B. J. Kim, H. Jin, S. J. Moon, J.-Y. Kim, B.-G. Park, C. S. Leem, J. Yu, T. W. Noh, C. Kim, S.-J. Oh, J.-H. Park, V. Durairaj, G. Cao, and E. Rotenberg, Phys. Rev. Lett. **101**, 076402 (2008).
[13] Y. Singh and P. Gegenwart, Phys. Rev. B **82**, 064412 (2010).
[14] S. K. Pandey and K. Maiti, Phys. Rev. B **82**, 035110 (2010).
[15] S. J. Moon, H. Jin, K. W. Kim, W. S. Choi, Y. S. Lee, J. Yu, G. Cao, A. Sumi, H. Funakubo, C. Bernhard, and T. W. Noh, Phys. Rev. Lett. **101**, 226402 (2008).
[16] B. J. Yang and Y. B. Kim, Phys. Rev. B **82**, 085111 (2010).
[17] C. H. Kim, H. S. Kim, H. Jeong, H. Jin, and J. Yu, Phys. Rev. Lett. **108**, 106401 (2012).
[18] J. M. Carter, V. V. Shankar, M. A. Zeb, and H. Y. Kee, Phys. Rev. B **85**, 115105 (2012).
[19] A. Shitade, H. Katsura, J. Kunes, X.-L. Qi, S.-C. Zhang, and N. Nagaosa, Phys. Rev. Lett. **102**, 256403 (2009).
[20] P. Hosur, S. A. Parameswaran, and A. Vishwanath, Phys. Rev. Lett. **108**, 046602 (2012).
[21] W. Witczak-Krempa and Y. B. Kim, Phys. Rev. B **85**, 045124 (2012).
[22] X. Wan, A. M. Turner, A. Vishwanath, and S. Y. Savrasov, Phys. Rev. B **83**, 205101 (2011).
[23] B. J. Kim, J. Yu, H. Koh, I. Nagai, S. I. Ikeda, S. J. Oh, and C. Kim, Phys. Rev. Lett. **97**, 106401 (2006).
[24] M. K. Crawford, M. A. Subramanian, R. L. Harlow, J. A. Fernandez-Baca, Z. R. Wang, and D. C. Johnston, Phys. Rev. B **49**, 9198 (1994).
[25] B. J. Kim, H. Ohsumi, T. Komesu, S. Sakai, T. Morita, H. Takagi, and T. Arima, Science **323**, 1329 (2009).
[26] G. Cao, J. Bolivar, S. McCall, J. E. Crow, and R. P. Guertin, Phys. Rev. B **57**, R11039 (1998).
[27] I. Dzylosinsky, J. Phys. Chem. Solids **4**,241 (1958).
[28] T. Moriya, Phys. Rev. **120**, 91 (1960).
[29] M. Ge, T. F. Qi, O. B. Korneta, D. E. De Long, P. Schlottmann, W. P. Crummett, and G. Cao, Phys. Rev. B **84**, 100402(R) (2011).
[30] S. Boseggia, H. C. Walker, J. Vale, R. Springell, Z. Feng, R. S. Perry, M. M. Sala, H. M. Rønnow, S. P. Collins, and D. F. McMorrow, J. Phys.: Condens. Matter **25**, 422202 (2013).
[31] H. Watanabe, T. Shirakawa, and S. Yunoki, Phys. Rev. Lett. **110**, 027002 (2013).
[32] J. S. Lee, Y. Krockenberger, K. S. Takahashi, M. Kawasaki, and Y. Tokura, Phys. Rev. B **85**, 035101 (2012).
[33] T. F. Qi, O. B. Korneta, L. Li, K. Butrouna, V. S. Cao, X. Wan, P. Schlottmann, R. K. Kaul, and G. Cao, Phys. Rev. B **86**, 125105 (2012).
[34] D. Haskel, G. Fabbris, M. Zhernenkov, P. P. Kong, C. Q. Jin, G. Cao, and M. van Veenendaal, Phys. Rev. Lett. **109**, 027204 (2012).

[35] J. Nichols, J. Terzic, E. G. Bittle, O. B. Korneta, L. E. De Long, J. W. Brill, G. Cao, and S. S. A. Seo, Appl. Phys. Lett. **102**, 141908 (2013).

[36] C. Rayan-Serrao, J. Liu, J. T. Heron, G. Singh-Bhalla, A. Yadav, S. J. Suresha, R. J. Paull, D. Yi, J.-H. Chu, M. Trassin, A. Vishwanath, E. Arenholz, C. Frontera, J. Železný, T. Jungwirth, X. Marti, and R. Ramesh, Phys. Rev. B **87**, 085121 (2013).

[37] C. C. Castaneda, G. Tavizon, A. Baeza, P. Mora, and R. Escudero, J. Phys.: Condens. Matter **19**, 446210 (2007).

[38] X. Marti, I. Fina, D. Yi, J. Liu, J. H. Chu, C. Rayan-Serrao, S. Suresha, J. Železný, T. Jungwirth, J. Fontcuberta, R. Ramesh, arXiv:1303.4704 (to be published).

[39] L. Miao, P. Silwal, X. Zhou, I. Stern, J. Peng, W. Zhang, L. Spinu, Z. Q. Mao, and D. H. Kim, Appl. Lett. Phys. **100**, 052401 (2012).

[40] J. Wolfman, W. Prellier, Ch. Simon, and B. Mercey, J. Appl. Phys. **83**, 7186 (1998).

[41] K. Jin, X. H. Zhang, P. Bach, and R. L. Greene, Phys. Rev. B **80**, 012501 (2009).

[42] H. Okabe, M. Isobe, E. Takayama-Muromachi, A. Koda, S. Takeshita, M. Hiraishi, M. Miyazaki, R. Kadono, Y. Miyake, and J. Akimitsu, Phys. Rev. B **83**, 155118 (2011).

[43] S. Boseggia, R. Springell, H. C. Walker, H. M. Rønnow, Ch. Rüegg, H. Okabe, M. Isobe, R. S. Perry, S. P. Collins, and D. F. McMorrow, Phys. Rev. Lett. **110**, 117207 (2013).